Schizophrenia polygenic risk during typical development reflects multiscale cortical organization

Matthias Kirschner[1,2*], Casey Paquola[1,3*], Budhachandra S. Khundrakpam[1], Uku Vainik[1,4], Neha Bhutani[1], Benazir-Hodzic-Santor, Noor B. Al-Sharif[1], Bratislav Misic[1], Boris Bernhardt[1], Alan C. Evans[1] and Alain Dagher[1]

*equal contribution

[1]Montreal Neurological Institute, McGill University, Montreal, QC, Canada

[2]Department of Psychiatry, Psychotherapy and Psychosomatics, Psychiatric Hospital, University of Zurich, Switzerland

[3]Institute of Neuroscience and Medicine (INM-1), Forschungszentrum Jülich, Jülich, Germany

[4]Institute of Psychology, Faculty of Social Sciences, Tartu, Estonia

Polygenic risk of schizophrenia and cortical morphometry in typically developing children

Abstract

Schizophrenia is widely recognized as a neurodevelopmental disorder, but determining neurodevelopmental features of schizophrenia requires a departure from classic case-control designs. Polygenic risk scoring for schizophrenia (PRS-SCZ) enables investigation of the influence of genetic risk for schizophrenia on cortical anatomy during neurodevelopment and prior to disease onset. PRS-SCZ and cortical morphometry were assessed in typically developing children (3 – 21 years) using T1-weighted MRI and whole genome genotyping (n=390) from the Pediatric Imaging, Neurocognition and Genetics (PING) cohort. Then, we sought to contextualise the findings using (i) age-matched transcriptomics, (ii) gradients of cortical differentiation and (iii) case-control differences of major psychiatric disorders. Higher PRS-SCZ was associated with greater cortical thickness in typically developing children, while surface area and cortical volume showed only subtle associations. Greater cortical thickness was most prominent in areas with heightened gene expression for dendrites and synapses. The pattern of PRS-SCZ associations with cortical thickness reflected functional specialisation in the cortex and was spatially related to cortical abnormalities of patient populations of schizophrenia, bipolar disorder, and major depression. Finally, age interaction models indicated PRS-SCZ effects on cortical thickness were most pronounced between ages 3 and 6, suggesting an influence of PRS-SCZ on cortical maturation early in life. Integrating imaging-genetics with multi-scale mapping of cortical organization, our work contributes to an emerging understanding of how risk for schizophrenia and related disorders manifest in early life.

Introduction

Schizophrenia is a multifaceted and highly heritable psychiatric disorder that is widely recognized to have a neurodevelopmental origin (Insel, 2010; Rapoport, Giedd and Gogtay, 2012; Birnbaum and Weinberger, 2017). Abnormal brain development likely predates the onset of clinical symptoms, which typically emerge in early adulthood (Kessler *et al.*, 2007). Genome-wide association studies (GWAS) support this hypothesis by showing schizophrenia-related genes are involved in multiple neurodevelopmental processes (Schizophrenia Working Group of the Psychiatric Genomics Consortium *et al.*, 2014; Birnbaum and Weinberger, 2017). These genes may affect brain development, leading to vulnerability to environmental effects, and have been suggested to contribute to atypical cortical morphology, as previously observed in cohorts with a schizophrenia diagnosis (Rapoport, Giedd and Gogtay, 2012).

Childhood and adolescent brain development involves dynamic and complex structural changes that are shaped by genetic and environmental factors (Shaw *et al.*, 2006, 2007; Raznahan *et al.*, 2011; Schmitt *et al.*, 2014; Khundrakpam *et al.*, 2017; Park *et al.*, 2021). Longitudinal neuroimaging studies have consistently reported a global increase in cortical volume, thickness, and surface area that typically peaks in late childhood and is followed by decreases in adolescence (Raznahan *et al.*, 2011; Wierenga *et al.*, 2014; Tamnes *et al.*, 2017). At the same time, regional maturational trajectories are heterochronous, whereby sensory areas mature earlier than transmodal cortex (Giedd *et al.*, 1999; Gogtay *et al.*, 2004; Sowell *et al.*, 2004), shaping large-scale patterns of cortical differentiation (Paquola, Bethlehem, *et al.*, 2019).

The neurodevelopmental hypothesis of schizophrenia posits that cortical maturation is perturbed, producing widespread cortical abnormalities (van Erp *et al.*, 2018). Differences in cortical morphometry are consistently reported across different stages and clinical phenotypes of the schizophrenia spectrum (Wannan *et al.*, 2019; Kirschner *et al.*, 2020, 2021; ENIGMA Clinical High Risk for Psychosis Working Group *et al.*, 2021). Investigating neurodevelopmental features of schizophrenia requires a departure from classic case-control designs, however. Alternatively, focusing on genetic risk enables us to investigate neuroanatomical correlates in a large population-based cohort of children and adolescents, without interacting disease-related factors (e.g. medication, chronicity). Recent work shows sensitivity of polygenic risk scoring for schizophrenia (PRS-SCZ) to cortical morphometry (French *et al.*, 2015; Liu *et al.*, 2017; Neilson *et al.*, 2017, 2019), though not necessarily grey

matter volume (Van der Auwera *et al.*, 2015; Auwera *et al.*, 2017; Reus *et al.*, 2017). Thus far, studies have centred almost exclusively on adult cohorts. Only one study has investigated adolescents (aged 12–21 years) (French *et al.*, 2015). Discerning neurodevelopmental aspects of genetic risk for schizophrenia requires investigation of younger cohorts.

Understanding the relation of genetic risk for schizophrenia to neurodevelopment can be further enhanced by contextualising the imaging-derived phenotype with maps of cortical organization. At the cellular level, a range of processes associated with healthy cortical development, such as synaptic pruning, dendritic arborization and intracortical myelination, are implicated in the development of schizophrenia and may produce regional cortical disruptions (Feinberg, 1982; Sellgren *et al.*, 2019; Sprooten *et al.*, 2019; Wei *et al.*, 2020). Recent advances in RNA sequencing (RNAseq) of post mortem brain tissue (Zhu *et al.*, 2018) allow discernment of the relative contribution of cell-types to patterns of atypical cortical morphometry (Seidlitz *et al.*, 2020; Writing Committee for the Attention-Deficit/Hyperactivity Disorder *et al.*, 2021). The imaging-derived phenotype of genetic risk can also be indicative of sensitivity of different cortical types, defined by their microstructural make-up (Barbas, 2015). At this microstructural level, cortical differentiation is related to graded changes in the thickness and density of cortical layers (Sanides, 1962; García-Cabezas, Hacker and Zikopoulos, 2020). By resolving these gradients in the human brain (Paquola, Wael, *et al.*, 2019), we may evaluate genetic risk for schizophrenia with respect to the microstructural topography of the cortex. Similarly, at the level of macro-scale brain functional, cortical gradients efficiently describe prominent organisational principles, providing a low-dimensional depiction of functional specialisation across the cortex (Margulies *et al.*, 2016; Huntenburg *et al.*, 2017; Paquola, Wael, *et al.*, 2019). Finally, population-level effects of schizophrenia and other major psychiatric disorders can be used to illustrate the concordance of genetic risk for schizophrenia with disorder-related neuroanatomical phenotypes. Specifically, it can be tested how the association between genetic risk of schizophrenia and cortical morphometry in children relates to shared and divergent neuroanatomical abnormalities across psychiatric disorders (Opel *et al.*, 2020; Writing Committee for the Attention-Deficit/Hyperactivity Disorder *et al.*, 2021). Taken together, multiple scales of cortical organisation can be utilized to provide a comprehensive description of the regional variations of an imaging-derived phenotype, such as genetic risk for schizophrenia.

Here we address the relationship between PRS-SCZ and cortical organization in a large population-based cohort of typically developing children (3 – 21 years) derived from the Pediatric Imaging, Neurocognition and Genetics (PING) study (Jernigan *et al.*, 2016). We hypothesised that higher PRS-SCZ would be associated with atypical cortical morphometry (thickness, surface area and volume). Then, we aimed to disambiguate the effect of PRS-SCZ on cortical morphometry by comparing the observed spatial patterns to cell type specific gene-expression, gradients of cortical differentiation, and cortical abnormalities seen in major psychiatric disorders. Finally, we examined age-specific variations in PRS-SCZ effects by simulating a trajectory of abnormal cortical development in high PRS-SCZ individuals.

Results

Polygenic risk for SCZ is associated with greater cortical thickness

To test the association between PRS-SCZ and cortical morphometry in typically developing children, we used T1-weighted MRI and whole genome genotyping (n=390) from the PING cohort (3–21 years, mean±sd = 12.1±4.7 years, 46% female) (**Table 1**). Vertex-wise general linear modelling (GLM) related cortical thickness with PRS-SCZ, controlling for age, sex, the first 10 principal components of genetic variants (to account for population stratification), scanner, and total brain volume. We found that higher PRS-SCZ was significantly associated with greater cortical thickness (Random Field Theory (RFT) corrected, $P < 0.01$) but not surface area or cortical volume (**Figure 1B, Supplementary Figures 2-3**). Overall, the unthresholded t-statistic map revealed that higher PRS-SCZ was associated with widespread increases in cortical thickness in association cortex, but reduced cortical thickness in sensory areas (**Figure 1C top; Supplementary Figure 1**). Higher PRS-SCZ was associated with significantly thicker cortex in the left insula, left superior temporal gyrus and left inferior parietal lobule (**Figure 1C bottom**, RFT corrected, $P<0.01$). These results suggest a significant effect of PRS-SCZ on cortical thickness but not surface area or cortical volume in typically developing children. As such, subsequent analysis are restricted to cortical thickness.

Spatial association with transcriptomic, macroscopic, and disorder-related patterns of cortical organization

In a next step, we sought to examine how PRS-SCZ effects on cortical thickness in typically developing children relate to different levels of cortical organization. The pattern of PRS-SCZ effects on cortical thickness were compared to 1) cell type specific gene expression 2)

microstructural and functional gradients and 3) cortical pattern of case-control differences from three major psychiatric disorders.

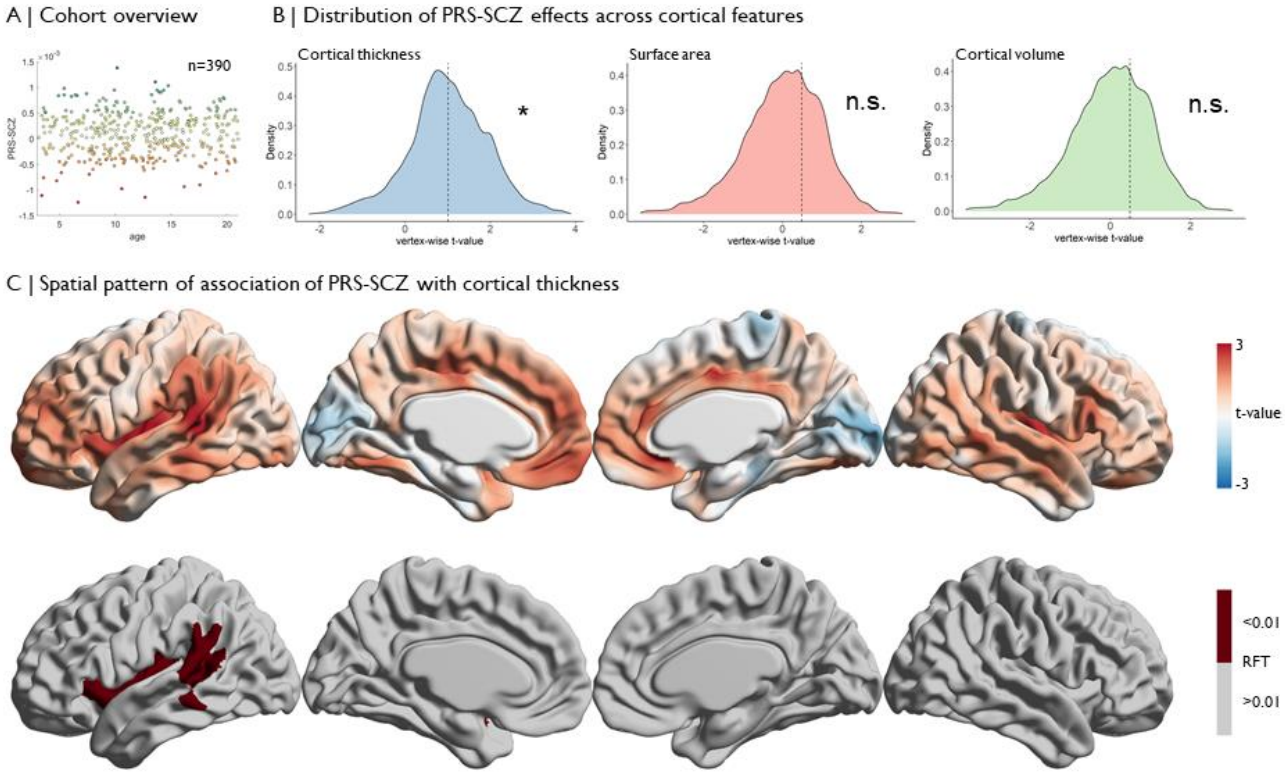

Figure 1: Association of PRS-SCZ with cortical morphometry. A) Scatterplot of PRS-SCZ scores by age within the selected cohort. **B)** Probability distributions show the variation in vertex-wise t-values of the association of PRS-SCZ with each cortical feature. Only cortical thickness is significantly shifted from 0. **C)** Unthresholded (top) and thresholded (bottom) maps show the association of PRS-SCZ with cortical thickness. Unthresholded maps for surface area and cortical volume are Supplementary Figures 2-3.

Alignment with cell-type specific gene expression

Histological examinations have reported a null or minimal relationship between cortical thickness and neuron number in healthy brain samples (Collins *et al.*, 2010; Cahalane, Charvet and Finlay, 2012; Carlo and Stevens, 2013). Instead, regional variations in cortical thickness show a strong association with neuropil (Carlo and Stevens, 2013), the portion of cortical tissue that excludes cell bodies or blood vessels (Braitenberg and Schüz, 1998). We examined whether cortical thickness differences related to PRS-SCZ mirrored regional variations in the neuropil composition of the cortex, in order to generate hypotheses on the neuropil components affected by PRS-SCZ. To this end, we first validated the relationship between cortical thickness and neuropil using tabular data and photomicrographs of Nissl stains [r=0.49, p_{spin}=.018, **Figure 2A**, (von Economo and Koskinas, 1925; Economo, 2009)].

Note that neuronal density was not correlated with histologically-defined cortical thickness (r=0.08 p_{spin}=.678), confirming previous work (Cahalane, Charvet and Finlay, 2012; Carlo and Stevens, 2013). Then, we estimated regional variations in neuropil-related gene expression, based on six cellular components (astrocytes, microglia, oligodendrocytes, axons, dendritic trees, neuron-to-neuron synapses) by combining tissue-level RNAseq with single-cell RNAseq for cell-types (Zhu *et al.*, 2018) and gene ontologies for neuron-compartments (Ashburner *et al.*, 2000; The Gene Ontology Consortium, 2019) (**Figure 2B**). Correlating PRS-SCZ effects on cortical thickness with neuropil-related gene expression, we found that PRS-SCZ effects are significantly associated with gene expression for dendritic trees (r=.755, p_{perm}=.006), synapses (r=.618, p_{perm}=.005), and at a trend-level with axons (r=.481, p_{perm}=.069) (**Figure 2C**). In contrast, no significant correlation was observed with gene expression related to glial components of neuropil (**Figure 2C**). Together, these analyses suggest greater cortical thickness with higher PRS-SCZ is observed in areas with greater dendritic and synaptic density.

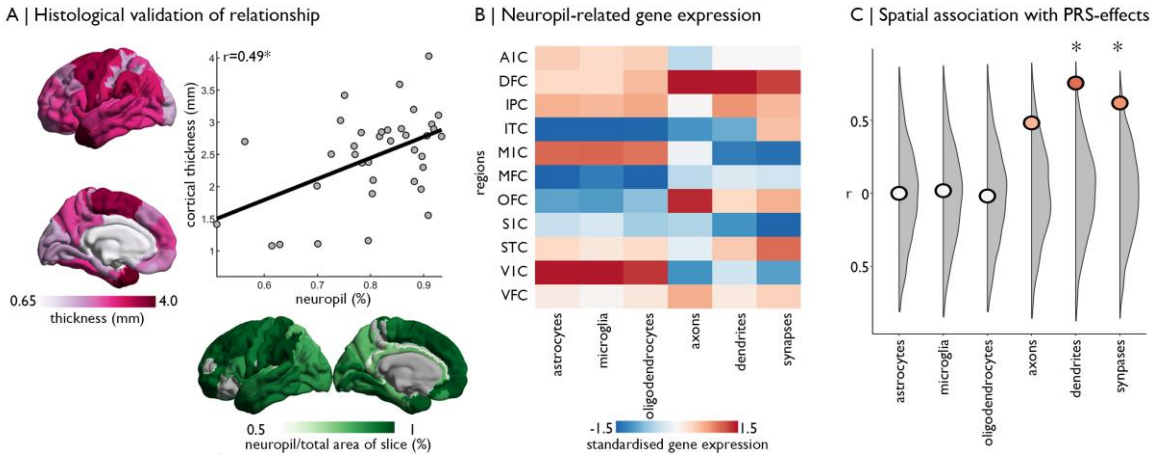

Figure 2: Decoding spatial patterns of PRS-SCZ on cortical thickness. A) Correlation of histological measurements of cortical thickness and neuropil (Von Economo & Koskinas, 1925). Cortical thickness is shown in pink and on the y-axis. Neuropil is shown in green and on the x-axis. **B)** Gene expression varies across glial and neuron-related compartments of neuropil in eleven cortical regions. **C)** Correlation of neuropil-related gene expression with the PRS-SCZ effects showed significant association with dendrites and synapses, compared with null distributions from permutation testing (grey). **Abbreviations**. A1C: primary auditory cortex. DFC: dorsal frontal cortex. IPC: inferior parietal cortex. ITC: inferior temporal cortex. M1C: primary motor cortex. MFC: medial frontal cortex. OFC: orbital frontal cortex. S1C: primary somatosensory cortex. STC: superior temporal cortex. V1C: primary visual cortex. VFC: ventral frontal cortex.

Contextualisation by microstructural and functional gradients

We assessed the concordance of PRS-SCZ effects on cortical thickness with system-level microstructural and functional differentiation. Microstructural and functional differentiation were represented by eigenvector decompositions of inter-regional correlations of microstructure-sensitive MRI (T1w/T2w) and resting-state functional MRI data in healthy adults (Paquola, Wael, *et al.*, 2019). Each eigenvector reflects a cortical gradient of a microstructural property or pattern of resting state functional connectivity. We used least absolute shrinkage and selection operator (LASSO) regression to determine the optimal combination of eigenvectors for models of increasing dimensionality. Higher regularisation in the LASSO regression forces small variable coefficients to zero (**Figure 3i**). The rankings of the eigenvectors reflect survival of the variable across regularisation, whereby the top ranked eigenvector has a non-zero coefficient at the highest regularisation. The two-dimensional models support visualisation of this modelling approach. For the microstructural model, PRS-SCZ-related greater cortical thickness is prominent on the lower half of eigenvector 1, comprising association cortex, whereas PRS-SCZ-related lower cortical thickness is observed in the lower right quadrant of the scatterplot, comprising occipital areas (**Figure 3Aii**). For the functional gradient model, PRS-SCZ-related greater cortical thickness is strongest in the upper right quadrant, involving inferior central and superior temporal areas (**Figure 3Bii**). Beyond anatomical localisation of the strongest effects, a key advantage of this framework is statistical evaluation of the best combination of eigenvectors. The explanatory power of the microstructural model plateaus at approximately 20% of variance and, given the Bayesian Information Criterion increases from four to five dimensions, the four-dimensional model could be selected as the optimal combination (**Figure 3Aiii**). In contrast, increasing dimensionality of the functional gradient model provides major gains with each additional eigenvector, reaching 68% of variance explained with all 10 eigenvectors (**Figure 3Biii**). Thus, the broad pattern of the PRS-SCZ effect is captured by few microstructural gradients, while fine-grained differences in the PRS-SCZ effect are related to a high degree of functional specialisation.

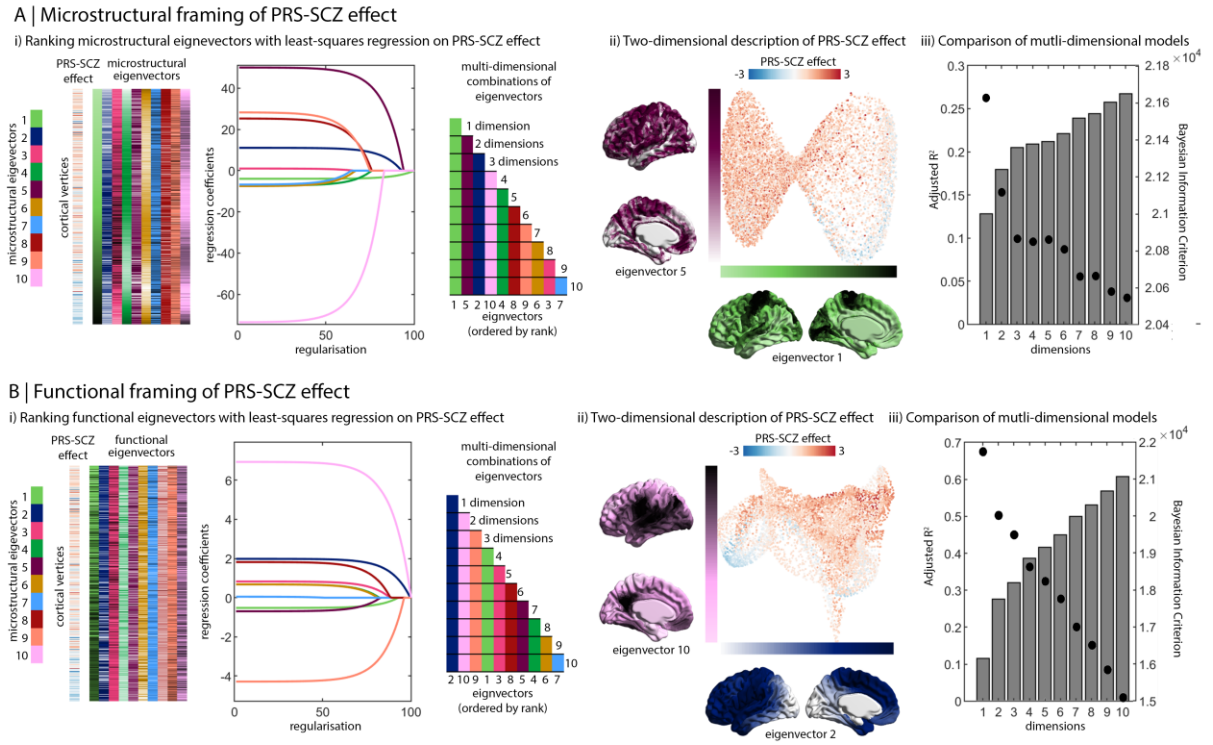

Figure 3: PRS-SCZ effect on cortical thickness framed by (A) microstructural and (B) functional gradients. i) Ten eigenvectors are investigated for each microstructural and functional differentiation. Eigenvectors represent the loading of a microstructural or functional component across the cortical surface. Line plots show the outcome of LASSO regression, with coefficients of each eigenvector sequentially forced to zero with increasing regularisation based on strength of association with PRS-SCZ effect on cortical thickness. The step plot shows the combinations of eigenvectors employed for multi-dimensional models. ii) Each dot in the scatter plot represents a cortical vertex and is coloured by PRS-SCZ effect on cortical thickness. The x- and y-axes are top-ranked eigenvectors, illustrating the variation in PRS-SCZ effect on cortical thickness in the context of these cortical gradients. iii) For each multi-dimensional combination shown in the step plot, we deployed a linear model with full interaction terms to explain variance in PRS-SCZ effect on cortical thickness. Bar plot shows the adjusted R^2 score of the model and scatter plot the Bayesian Information Criterion.

Cortical thickness signatures of PRS-SCZ and major psychiatric disorders

We assessed whether PRS-SCZ effects on cortical thickness relate to patterns of cortical thickness abnormalities observed in schizophrenia and other psychiatric illnesses. We made use of recent adult case-control meta-analyses and mega-analysis from the ENIGMA consortium in schizophrenia (van Erp *et al.*, 2018), bipolar disorder (Hibar *et al.*, 2018), major depressive disorder (Schmaal *et al.*, 2017), attention deficit hyperactivity disorder (Hoogman *et al.*, 2019), obsessive compulsive disorder (Boedhoe *et al.*, 2017) and autism spectrum disorder (van Rooij *et al.*, 2018), which are available in our open access ENIGMA toolbox (Lariviere *et al.*, 2020). To this end, the PRS-SCZ related t-statistic map was parcellated into 64 Desikan-Killiany (DK) atlas regions (Desikan *et al.*, 2006), and correlated

with the case-control Cohen's d-map for each condition and statistically evaluated relative to 10,000 null models. The null models account for spatial autocorrelation by randomly spinning one map across the cortical surface. We identified negative correlations between the PRS-SCZ effects on cortical thickness and disorder-related cortical abnormalities (case-control Cohen's d-maps) in schizophrenia (r=-.326, p_{spin}=.0022). In addition, we found similar negative correlations to cortical abnormalities in bipolar disorder (r=-.466, p_{spin}<.001), major depressive disorder (r=-.538, p_{spin}<.001) and attention deficit hyperactivity disorder (r=-.430, p_{spin}<.001) but not obsessive compulsive disorder or autism spectrum disorder (**Figure 4**). Cortical regions showing PRS-SCZ related greater thickness are those with the strongest thinning across disease maps of schizophrenia and genetically related psychiatric disorders such as bipolar disorder, depression and attention deficits hyperactivity disorder.

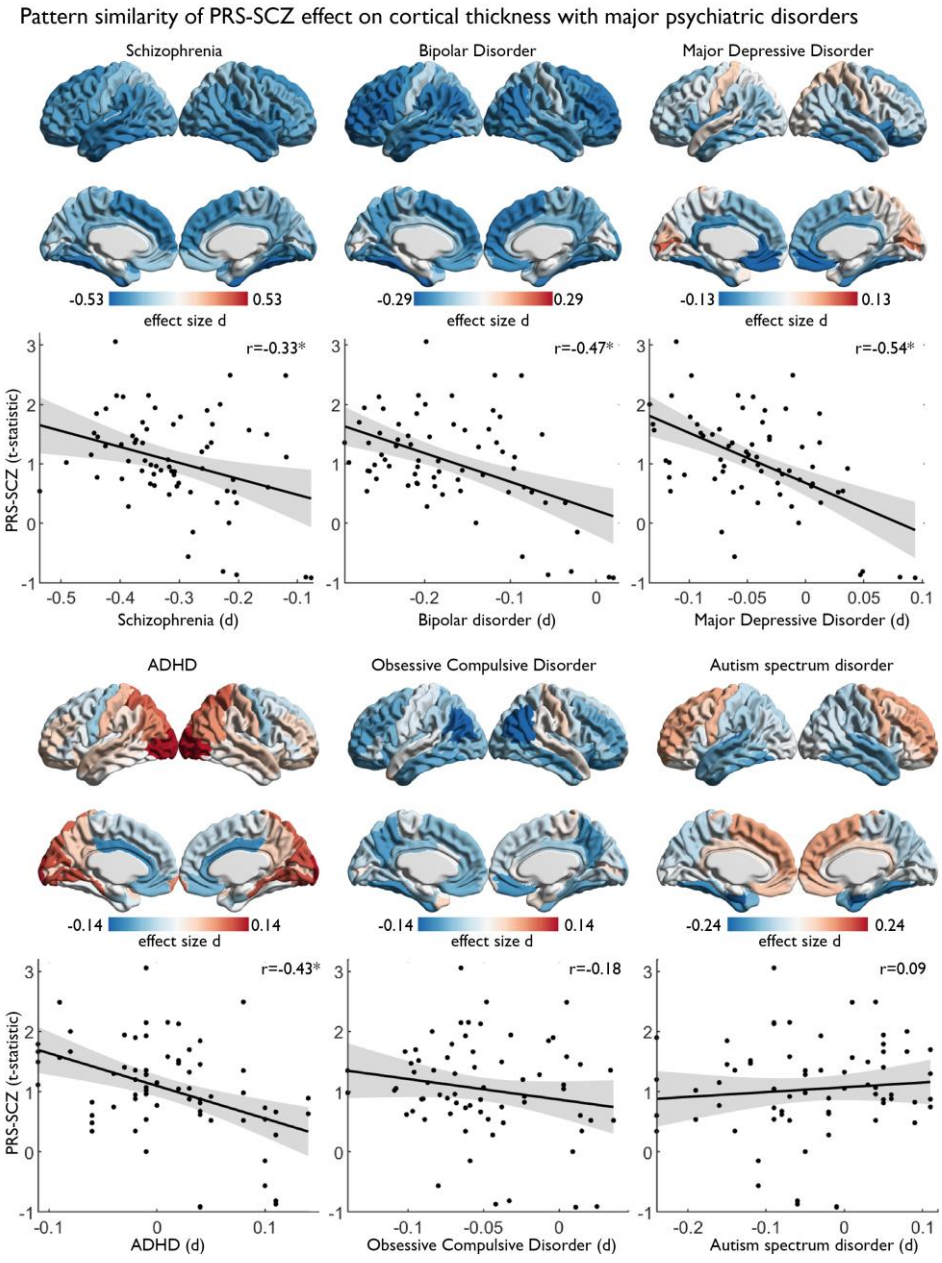

Figure 4: Pattern similarity of PRS-SCZ on cortical thickness with major psychiatric disorders. Cortical surfaces show the effect size of schizophrenia, bipolar disorder and major depressive disorder, attention deficit hyperactivity disorder, obsessive compulsive disorder and autism spectrum disorder diagnosis on cortical thickness from mega-analyses of each disorder (Lariviere *et al.*, 2020). Scatterplots show the correlation of each map with PRS-SCZ effect on cortical thickness.

Age-centred effects of PRS-SCZ

Schizophrenia-related genes are implicated in neurodevelopmental processes and as such the effect of PRS-SCZ on cortical thickness likely varies with age. Although the cross-sectional nature of this cohort prohibits mapping individual trajectories of cortical development, we sought to approximate developmental variation in the effect of PRS-SCZ by estimating age-specific effects in the cohort (Khundrakpam *et al.*, 2017). To this end, we centered age in 1-year intervals between 3 and 21 years and repeated the GLM predicting cortical thickness with PRS-SCZ. By shifting the distribution of the age term, the model approximates the PRS-SCZ effect on cortical thickness at each centred year. We found that higher PRS-SCZ was associated with greater cortical thickness during age 3 to age 6 (**Figure 5A**, see **Supplementary Figure 4 and 5**for RFT corrected maps and all age bins) closely resembling the results from the main analysis (**Figure 1C**). After age 6, the effect changed sign, and higher PRS-SCZ correlated with reduced cortical thickness during age 9 to 18, while between age 19 and 21 the PRS-SCZ effects on cortical thickness returned to a similar pattern as in age 3 to 6. These findings suggest more pronounced PRS-SCZ effects on cortical thickness in early childhood.

Finally, we tested whether age-variant PRS-SCZ effects were reflective of distinct transcriptomic, macroscale and disorder-related patterns of cortical organisation. Spatial patterns of gene expression related to dendrites and synapses overlapped significantly with PRS-SCZ effects from 3-8 and 3-7 years, respectively (all $r>0.64$, $p_{perm}<.025$), whereas axon-related gene expression exhibited a negative correlation with PRS-SCZ effects at 15, 17 and 18 years (all $r<-0.60$, $p_{perm}<.025$; **Figure 5Bi**). No significant correlations were observed with glia-related gene expression. Microstructural and functional gradients best accounted for PRS-SCZ effects at the earliest ages (**Figure 5Bii**). Finally, PRS-SCZ effects were associated with disorder-related cortical abnormalities across the age range, however, the correlation flipped from childhood to adolescence. Specifically, PRS-SCZ related increase in cortical thickness during 3-6 years showed negative correlations with cortical abnormalities of schizophrenia and related major psychiatric disorders (all $r<-0.25$, $p_{spin}<.025$), whereas PRS-

SCZ related reduced cortical thickness in the 12-15 year age range was positively correlated with cortical abnormalities of bipolar disorder and negatively with autism spectrum disorder (all r>0.25, p_{spin}<.025, **Figure 5Biii**). Together, these analyses emphasise the distinctiveness of childhood vs adolescent effects of PRS-SCZ on cortical thickness.

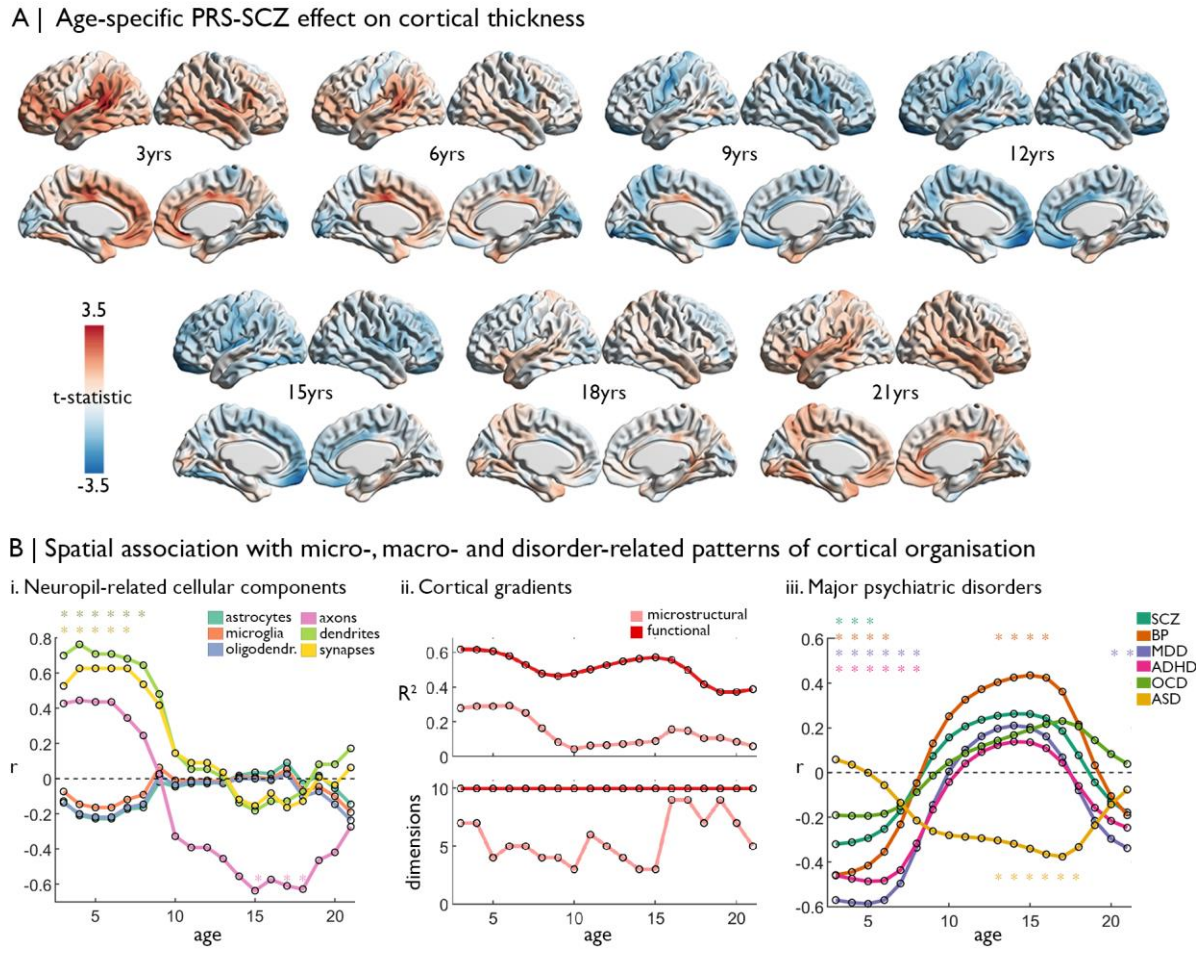

Figure 5: Age-specific PRS-SCZ effect on cortical thickness. A) Unthresholed maps of PRS-SCZ effect on cortical thickness with different age-centering. **B)** Pattern similarity of age-specific maps with neuropil-related gene expression (Figure 2), cortical gradients (Figure 3) and major psychiatric disorders (Figure 4).

Discussion

Combining imaging-genetics with multi-scale mapping, we characterised the relation of PRS-SCZ on cortical morphometry across different scales of cortical organization. We found that higher PRS-SCZ was associated with greater cortical thickness in typically developing children, while surface area and cortical volume showed only subtle associations with PRS-SCZ. Furthermore, we provide evidence that PRS-SCZ preferentially affects areas with heightened expression of dendrites and synapses and that the PRS-SCZ related cortical pattern is captured by functional specialisation in the cortex. We also find that the PRS-SCZ

related cortical pattern mirrors cortical thinning related to schizophrenia and other major psychiatric disorders. Finally, age-centred models suggest that PRS-SCZ effects on cortical thickness are most prominent between ages 3 and 6.

Our cell-type specific gene expression approach enabled cross-modal exploration of the relationship of genetic risk for schizophrenia with expression levels of neurons and glia. Our findings support and extend upon post-mortem analyses, which demonstrate abnormal dendritic and synaptic density in individuals with schizophrenia (see (Berdenis van Berlekom *et al.*, 2020) for a recent meta-analysis). Another recent study showed that differences in cortical thickness across multiple psychiatric disorders (including schizophrenia) are associated with pyramidal-cell gene expression, a gene set enriched for biological processes of dendrites (e.g. dendritic arborization and branching) (Srinivas *et al.*, 2017) as well as synaptic function (Writing Committee for the Attention-Deficit/Hyperactivity Disorder *et al.*, 2021). While those authors reported an involvement of astrocytes and microglia for cross-disorder effects, our findings point towards a specific relationship between gene expression of dendrites and synapses with PRS-SCZ related cortical differences during neurodevelopment.

The sensitivity of different cortical regions to PRS-SCZ effects were also related to microstructural and functional features. Notably, the dimensionality of the optimal models differed between the modalities. Few microstructural gradients were needed to explain significant variance in the PRS-SCZ effects, the strongest of which was the principal microstructural gradient (Paquola, 2019). Thus, alignment with this well-established sensory-fugal axis may be used to infer that areas with higher plasticity, such as paralimbic and temporal areas (García-Cabezas *et al.*, 2017), are particularly vulnerable to the genetic risk of schizophrenia. However, microstructural gradient model performance quickly plateaued with increasing dimensionality, suggesting that only the general pattern could be captured by microstructural differentiation. In contrast, performance of the functional gradient model improved with higher dimensionality, towards a very high level of variance explained in the PRS-SCZ effects. This shows that nuances in the PRS-SCZ related cortical pattern may be related to functional specialisation.

We observed that the PRS-SCZ effects on cortical thickness appear to be transient and disappear with cortical maturation in typically developing children and adolescents; however, we presume that they may persist or worsen in the presence of other biological and

environmental risk factors. Several longitudinal and case-control studies have shown that the development of psychosis in high-risk adolescents is associated with progressive loss of cortical thickness in several areas of association cortex (Pantelis *et al.*, 2003; Cannon *et al.*, 2015; ENIGMA Clinical High Risk for Psychosis Working Group *et al.*, 2021). Of note, the areas implicated in these studies overlap considerably with those showing increased cortical thickness with higher PRS-SZ here. We further observed that the pattern of PRS-SCZ related cortical thickening was associated with areas of cortical thinning in schizophrenia, bipolar disorder, major depression and attention deficit hyperactive disorder. This transdiagnostic overlap echoes the genetic and phenotypic correlation between these disorders (ReproGen Consortium *et al.*, 2015; Consortium *et al.*, 2018; Opel *et al.*, 2020; Writing Committee for the Attention-Deficit/Hyperactivity Disorder *et al.*, 2021). While we do not know the cause of increased cortical thickness in our sample, converging evidence supports the idea that reduced cortical thickness in schizophrenia results from loss of neuropil, and specifically synapses. For example, post mortem studies in schizophrenia demonstrate synaptic loss (Berdenis van Berlekom *et al.*, 2020); many genes implicated in schizophrenia are associated with synapses or synaptic pruning (Kirov *et al.*, 2012; Schizophrenia Working Group of the Psychiatric Genomics Consortium *et al.*, 2014; Consortium *et al.*, 2020); regional variations in cortical thickness correlate with neuropil (Carlo and Stevens, 2013). It is conceivable that the PRS-SCZ is associated with delayed pruning and an excess of synapses for age, which in turn may render the affected brain regions vulnerable to catastrophic synaptic loss during the emergence of psychosis.

The association of PRS-SCZ with greater cortical thickness in childhood raises the question of how the genetic risk of schizophrenia contributes to abnormal developmental trajectories. The age-centred analyses showed that the PRS-SCZ signature of greater cortical thickness was most prominent from 3 to 6 years. Given that the transmodal areas identified in the present analysis, such as the insula, exhibit modest cortical thinning from 3-21 years (Zielinski *et al.*, 2014; Sotiras *et al.*, 2017; Ball, Beare and Seal, 2019), our results align with either an amplified trajectory (ie: higher peak, steeper decline) and/or delayed cortical thinning in early childhood. Related to the complexity and heterochronicity of cortical maturation during childhood and adolescents (Ball, Beare and Seal, 2019), polygenic disorders can involve multiple types of abnormal trajectories, occurring simultaneously or sequentially (Di Martino *et al.*, 2014; Klingler *et al.*, 2021). Amplified or delayed trajectory of transmodal area morphometry may represent a core motif of cortical development in

children with high PRS-SCZ. The PRS-SCZ includes multiple genetic factors, however, and their individual variation may produce heterogeneity in cortical development within high PRS-SCZ individuals. The present study has to be interpreted in the light of the cross-sectional nature of the dataset that has limited the ability to map individual longitudinal trajectories. Research could be enhanced by larger datasets with longitudinal designs and longer follow-up to determine which individuals will develop psychosis or other mental disorders. Our results point towards specific effects of PRS-SCZ on cortical thickness in early childhood (age 3 to 6) highlighting the need for large-scale initiatives targeting this age range.

Conclusions

The present study illustrates how maps of cortical organization can enrich descriptions of imaging-derived phenotypes related to genetic risk for mental illnesses. In this case, contextualisation provided novel evidence on cellular basis and developmental trajectory of genetic risk for schizophrenia on cortical thickness. This work may help to refine the neurodevelopmental hypothesis of schizophrenia. More generally, the present work provides an integrative framework combining imaging-genetics and multi-scale mapping that could advance our understanding of the complex associations between individual genetic profiles and cortical organization across multiple psychiatric and neurological conditions.

Material and Methods

Subjects

Neuroimaging, demographic and genetic data of typically developing children and adolescents were derived from the PING study (Jernigan *et al.*, 2016). The PING dataset is a wide-ranging, publicly shared data resource comprising cross-sectional data from 1493 healthy subjects evaluated at 10 different sites across the United States. Details of the PING dataset are described elsewhere (Jernigan *et al.*, 2016).

Genomic data

Genomic data processing and calculation of polygenic risk scores followed a recent publication from Khundrakpam and colleagues (Khundrakpam *et al.*, 2020). Specifically, 550,000 single nucleotide polymorphisms (SNPs) were genotyped from saliva samples using the Illumina Human660W-Quad BeadChip. Data were prepared for imputation using the "imputePrepSanger" pipeline (https://hub.docker.com/r/eauforest/imputeprepsanger/), implemented on CBRAIN (Sherif et al., 2014) and the Human660W-Quad_v1_A-b37-strand

chip as reference. Taking Plink genotype files, the pipeline adjusted the strand, the positions, the reference alleles to match HRC panel, performed quality control steps and output a vcf file. The Plink quality control steps ensured that enough data were available for subjects and SNPs (--mind 0.1, --geno 0.1) and kept only common SNPs (--maf 0.05) that have passed the Hardy-Weinberg equilibrium test (-- hwe 5e-8). Indels, palindromic SNPs, SNPs with differing alleles, SNPs with no match to the reference panel, SNPs with > 0.2 allele frequency difference to the reference, and duplicates were also removed from the pipeline. The Sanger Imputation Service (McCarthy *et al.*, 2016) was used for data imputation, applying default settings and the Haplotype Reference Consortium, HRC (http://www.haplotype-reference-consortium.org/) as the reference panel. The imputed SNPs were further filtered with Plink v1.90b6.17 and v2.00a3LM (Chang *et al.*, 2015). All imputed SNPs had INFO scores R^2>0.9 and were filtered again using a more stringent filtration criteria (–mind 0.05, --geno 0.05, --maf 0.05, --hwe 1e6, --maf 0.05, --max-alleles 2) and heterozygosity rates (--het) 3 standard deviation (SD) units from the mean. We further omitted data from MHC complex (chr6 28477797 33448354 , https://www.ncbi.nlm.nih.gov/grc/human/regions/MHC?asm=GRCh37). After these processing steps, 4,673,732 variants were available for calculation of polygenic scores. Participants were filtered to have 0.95 loadings to the European genetic ancestry factor (coded as “GAF_europe” in the PING dataset), resulting in 526 participants. To model population structure, the same participants were used to calculate the 10 principal components across the variants, excluding areas in high LD with each other (--indep-pairwise 50 5 0.2) with Plink 2.

The PRS-SCZ was trained using results from latest GWAS on schizophrenia at the time of analysis (Ruderfer *et al.*, 2018). The GWAS was filtered for having imputation quality over 90. Polygenic scores were calculated with PRSice 2.30e (Choi and O’Reilly, 2019). We clumped the data as per PRSice default settings (clumping distance = 250kb, threshold r2 = 0.1), using the GWAS hits ($p< 5x10^{-08}$) cutoff criterion. After matching with available variants in the data, the PRS-SCZ was based on 87 variants.

Image acquisition and pre-processing

Details on image acquisition and pre-pre-processing are described elsewhere (Jernigan *et al.*, 2016). Each site administered a standardized structural MRI protocol including a 3D T1-weighted inversion prepared RF-spoiled gradient echo scan using prospective motion correction (PROMO), for cortical and subcortical segmentation. The CIVET processing pipeline, (http://www.bic.mni.mcgill.ca/ServicesSoftware/CIVET, page 2.1) (Ad-Dab’bagh *et al.*, 2006), developed at the Montreal Neurological Institute, was used to compute cortical

thickness, surface area and cortical volume measurements at 81,924 regions covering the entire cortex (see supplementary methods for details). Quality control (QC) of these data was performed by two independent reviewers. Data with motion artifacts, a low signal to noise ratio (lower than 800), artifacts due to hyperintensities from blood vessels, surface-surface intersections, or poor placement of the grey or white matter (GM and WM) surface for any reason were excluded.

Of the total 526 subjects that passed filtering for European genetic ancestry. Next, filtering for individuals with information for demographics (age, sex, ethnicity and scanner) and those which passed quality control, resulted in a final sample of 390 participants. Demographic data from the 390 resulting participants from the PING dataset are described in Table 1.

Statistical analyses

Association between PRS-SCZ and cortical morphometry

To identify the association between PRS-SCZ on vertex-wise cortical thickness, surface area and cortical volume, general linear models (GLM) were applied using the SurfStat toolbox (http://www.math.mcgill.ca/keith/surfstat/) (Worsley *et al.*, 2009). Each cortical feature was modelled as:

$$T_i = \text{intercept} + \beta_1\text{PRS-SCZ} + \beta_2\text{Age} + \beta_3\text{Age}^2 + \beta_4\text{PRS-SCZ*Age} + \beta_5\text{PRS-SCZ*Age}^2 + \beta_6\text{Sex} + \beta_7\text{PC10} + \beta_8\text{Scanner} + \beta_9\text{BrainVolume} + \varepsilon_i \quad \text{(Eq.1)}$$

where *i* is a vertex, PRS-SCZ is the polygenic risk score for schizophrenia, *Age* is age in years at the time of scan, PC10 are the first 10 principal components of genomic data to account for population stratification, ε is the residual error, and the intercept and the β terms are the fixed effects. Please note, that models with quadratic age terms fit the data better than models with only lower degree age terms based on the corrected Akaike information criterion (AIC) and Bayesian information criterion (BIC) (supplementary methods). For each cortical feature, vertex-wise *t*-statistics of the association with PRS-SCZ (β_1PRS-SCZ) were mapped onto a standard surface. To assess the significance of PRS-SCZ effects on each of the three different cortical features whole brain correction for multiple comparisons using Random field theory (RFT) at cluster-level $p \leq .01$ (Hayasaka *et al.*, 2004; Worsley *et al.*, 2004) was applied. Please note, that only cortical thickness showed a significant association with PRS-SCZ after RFT correction (see results, Figure 1), thus all subsequent analyses were restricted to cortical thickness only.

Cellular composition of the cortex and PRS-SCZ effects on cortical thickness

We evaluated how the observed pattern of PRS-SCZ effects on cortical thickness relates to regional variations in the cellular compositions of the cortex. It is reported that regional variations in cortical thickness are not associated with the number of neurons (Herculano-Houzel, Watson and Paxinos, 2013). To further test this, we contrasted histological measurements of cortical thickness, neuronal density and neuropil (von Economo and Koskinas, 1925). Cortical thickness and neuronal density were retrieved from table data on 39 cortical areas. Neuropil was estimated by scanning Von Economo photomicrographs and calculating the proportion of non-stained pixels within each cortical area. Subsequently, we focused on components of the neuropil, namely glial cell processes, axons, dendritic trees, neuron-to-neuron synapses i.e. in cortical tissue other than cell bodies or blood vessels. Neuropil-related gene expression was calculated by combining tissue-level RNAseq with single-cell RNAseq for cell-types (Zhu *et al.*, 2018) and gene ontologies for neuron-compartments (Ashburner *et al.*, 2000; The Gene Ontology Consortium, 2019). Tissue-level RNAseq provided expression levels of 60,155 genes in 11 neocortical areas. The areas were cytoarchitecturally defined in each specimen, supporting precise mapping and comparison across individuals. Crucially, we selected 12 brain specimens that were age-matched to the imaging cohort (3-21 years), because gene expression differs substantially between children and adults (Kang *et al.*, 2011). Single-cell RNAseq provided specificity scores for each gene to glial cell types. For each type, we weighted the genes by the specificity score, then calculated the average across genes, across specimens and within area. For each neuron-compartment, we defined a list of marker genes using The Gene Ontology knowledgebase, then calculated the average expression of marker genes in each area and specimen. The annotated terms used were “neuron_to_neuron_synapse”, “dendritic_tree” and “main_axon”. Next, we mapped the 11 areas to the cortical surface and extracted area-average PRS-SCZ effects on cortical thickness. The cortical areas were visually matched to nearest parcel in a 200 parcel decomposition of the Desikan-Killany, as performed in previous work (Paquola *et al.*, 2020). Finally, we tested the spatial similarity of cell-type specific gene expression with PRS-SCZ effects on cortical thickness using product-moment correlations. Statistical significance was determined relative to random reassignment permutation tests (10,000 repetitions).

Microstructural and functional principal gradients and PRS-SCZ effects on cortical thickness

Microstructural and functional gradients were derived from Paquola and colleagues using the Human Connectome Project cohort (Paquola, Wael, *et al.*, 2019). In brief, microstructure profiles, reflecting T1w/T2w intensity sampled in the direction of cortical columns, were cross-correlated to estimate microstructural similarity across the cortex. The microstructural similarity matrix was subjected to diffusion map embedding, a nonlinear dimensionality reduction technique, to extract the top 10 eigenvectors of microstructural differentiation (Paquola, Wael, *et al.*, 2019). Cortex-wide resting state functional connectivity was also subjected to diffusion map embedding to identify top 10 eigenvectors of functional differentiation. Next, we used least absolute shrinkage and selection operator (LASSO) regression models to rank the eigenvectors by order of importance in explaining the PRS-SCZ effect on cortical thickness. Eigenvectors were ranked according to number of non-zero coefficient across 100 regularisation parameters, where only the highest regularisation resulted in all zero coefficients. Then, we used multiple linear regression models with increasing number of eigenvectors and full interaction terms to explain variance PRS-SCZ effect on cortical thickness. We evaluated the fit of the models based on the Bayesian Information Criterion and adjusted R^2.

Pattern similarity between PRS-SCZ effects and cortical abnormalities in major psychiatric disorders

We assessed whether cortical thickness differences of PRS-SCZ relate to patterns of cortical thickness abnormalities observed in major psychiatric disorder including schizophrenia, bipolar disorder, major depressive disorders, attention deficit hyperactivity disorder, autism spectrum disorder, obsessive compulsive disorder. To this end, the PRS-SCZ related t-statistic map was parcellated into 64 Desikan-Killiany (DK) atlas regions (Desikan *et al.*, 2006) and then correlated with the corresponding Cohen's d maps derived from recently published meta-analyses by the ENIGMA schizophrenia (van Erp *et al.*, 2018), bipolar disorder (Schmaal *et al.*, 2017), major depressive disorder working groups (Hibar *et al.*, 2018), attention deficit hyperactivity disorder (Hoogman *et al.*, 2019), obsessive compulsive disorder (Boedhoe *et al.*, 2017) and autism spectrum disorder (van Rooij *et al.*, 2018). implemented in the ENIGMA toolbox (Lariviere *et al.*, 2020). Specifically, spatial pattern similarity of cortical DK maps was examined using Pearson correlations following recently published approaches (Sun *et al.*, 2018; Larivière *et al.*, 2020). Statistical significance and correction of spatial autocorrelation were assessed with the spin permutation tests (10,000 repetitions) (Alexander-

Bloch *et al.*, 2018) following recent work from the ENIGMA Epilepsy Group (Larivière *et al.*, 2020) and implemented in the ENIGMA toolbox (Lariviere *et al.*, 2020). Of note, the medial wall was assigned as a NaN and not included in each the permuted correlation (Markello and Misic, 2020).

Age-centered effects of PRS-SCZ on cortical thickness

Age-specific associations between PRS-SCZ and cortical thickness were examined. To this end, we modified the abovementioned GLM (Eq.1) to use age centered in 1-year intervals between 3 and 21 years (Khundrakpam *et al.*, 2017). By shifting the distribution of the age term, the model approximates the PRS-SCZ effect on cortical thickness at the centred year (e.g. age 3). Each t-map was corrected for multiple comparison using RFT at $p \leq .01$ and $p \leq .05$ to identify those age bins with the strongest PRS-SCZ effects on cortical thickness. Note that there was no correlation between age and PRS-SCZ scores (r=0.058), which could have affected the age-centered analyses (Figure 1A). Finally, we evaluated how the age-specific pattern of PRS-SCZ effects on cortical thickness relates to multiscale and multilevel data of cortical organization. To this end, we repeated the correlation analysis with 1) cell type specific gene expression 2) microstructural and functional gradients and 3) cortical pattern of case-control studies from three major psychiatric disorders. To illustrate the association between age-centered PRS-SCZ effects on cortical thickness of all age bins (3 to 21 years) and each set of data (gene expression, gradients, case-control) caterpillar plots were used (Figure 3B).

Conflicts of interests

No conflicts of interest to report.

Acknowledgments

NBA is supported by grants from Brain Canada (238990, 243030), CFREF/HBHL Innovative Ideas (247613), Coutu Research Fund (241177), CFREF/HBHL Discovery (247712).

References

Ad-Dab'bagh, Y. *et al.* (2006) 'The CIVET Image-Processing Environment: A Fully Automated Comprehensive Pipeline for Anatomical Neuroimaging Research', in. *In Proceedings of the 12th Annual Meeting of the Organization for Human Brain Mapping*, p. 1.

Alexander-Bloch, A. F. *et al.* (2018) 'On testing for spatial correspondence between maps of human brain structure and function', *NeuroImage*, 178, pp. 540–551. doi: 10.1016/j.neuroimage.2018.05.070.

Ashburner, M. *et al.* (2000) 'Gene Ontology: tool for the unification of biology', *Nature Genetics*, 25(1), pp. 25–29. doi: 10.1038/75556.

Auwera, S. V. der *et al.* (2017) 'Predicting brain structure in population-based samples with biologically informed genetic scores for schizophrenia', *American Journal of Medical Genetics Part B: Neuropsychiatric Genetics*, 174(3), pp. 324–332. doi: https://doi.org/10.1002/ajmg.b.32519.

Ball, G., Beare, R. and Seal, M. L. (2019) 'Charting shared developmental trajectories of cortical thickness and structural connectivity in childhood and adolescence', *Human Brain Mapping*, 40(16), pp. 4630–4644. doi: 10.1002/hbm.24726.

Barbas, H. (2015) 'General Cortical and Special Prefrontal Connections: Principles from Structure to Function', *Annual Review of Neuroscience*, 38(1), pp. 269–289. doi: 10.1146/annurev-neuro-071714-033936.

Berdenis van Berlekom, A. *et al.* (2020) 'Synapse Pathology in Schizophrenia: A Meta-analysis of Postsynaptic Elements in Postmortem Brain Studies', *Schizophrenia Bulletin*, 46(2), pp. 374–386. doi: 10.1093/schbul/sbz060.

Birnbaum, R. and Weinberger, D. R. (2017) 'Genetic insights into the neurodevelopmental origins of schizophrenia', *Nature Reviews. Neuroscience*, 18(12), pp. 727–740. doi: 10.1038/nrn.2017.125.

Boedhoe, P. S. W. *et al.* (2017) 'Cortical Abnormalities Associated With Pediatric and Adult Obsessive-Compulsive Disorder: Findings From the ENIGMA Obsessive-Compulsive Disorder Working Group', *American Journal of Psychiatry*, 175(5), pp. 453–462. doi: 10.1176/appi.ajp.2017.17050485.

Braitenberg, V. and Schüz, A. (1998) 'Density of Axons', in Braitenberg, V. and Schüz, A. (eds) *Cortex: Statistics and Geometry of Neuronal Connectivity*. Berlin, Heidelberg: Springer Berlin Heidelberg, pp. 39–42. doi: 10.1007/978-3-662-03733-1_7.

Cahalane, D. J., Charvet, C. J. and Finlay, B. L. (2012) 'Systematic, balancing gradients in neuron density and number across the primate isocortex', *Frontiers in Neuroanatomy*, 6. doi: 10.3389/fnana.2012.00028.

Cannon, T. D. *et al.* (2015) 'Progressive Reduction in Cortical Thickness as Psychosis Develops: A Multisite Longitudinal Neuroimaging Study of Youth at Elevated Clinical Risk', *Biological Psychiatry*, 77(2), pp. 147–157. doi: 10.1016/j.biopsych.2014.05.023.

Carlo, C. N. and Stevens, C. F. (2013) 'Structural uniformity of neocortex, revisited', *Proceedings of the National Academy of Sciences*, 110(4), pp. 1488–1493. doi: 10.1073/pnas.1221398110.

Chang, C. C. *et al.* (2015) 'Second-generation PLINK: rising to the challenge of larger and richer datasets', *GigaScience*, 4, p. 7. doi: 10.1186/s13742-015-0047-8.

Choi, S. W. and O'Reilly, P. F. (2019) 'PRSice-2: Polygenic Risk Score software for biobank-scale data', *GigaScience*, 8(7). doi: 10.1093/gigascience/giz082.

Collins, C. E. *et al.* (2010) 'Neuron densities vary across and within cortical areas in primates', *Proceedings of the National Academy of Sciences of the United States of America*, 107(36), pp. 15927–15932. doi: 10.1073/pnas.1010356107.

Consortium, T. B. *et al.* (2018) 'Analysis of shared heritability in common disorders of the brain', *Science*, 360(6395). doi: 10.1126/science.aap8757.

Consortium, T. S. W. G. of the P. G. *et al.* (2020) 'Mapping genomic loci prioritises genes and implicates synaptic biology in schizophrenia', *medRxiv*, p. 2020.09.12.20192922. doi: 10.1101/2020.09.12.20192922.

Desikan, R. S. *et al.* (2006) 'An automated labeling system for subdividing the human cerebral cortex on MRI scans into gyral based regions of interest', *NeuroImage*, 31(3), pp. 968–980. doi: 10.1016/j.neuroimage.2006.01.021.

Di Martino, A. *et al.* (2014) 'Unraveling the Miswired Connectome: A Developmental Perspective', *Neuron*, 83(6), pp. 1335–1353. doi: 10.1016/j.neuron.2014.08.050.

von Economo, C. F. and Koskinas, G. N. (1925) *Die cytoarchitektonik der hirnrinde des erwachsenen menschen*. J. Springer.

Economo, C. von (2009) *Cellular Structure of the Human Cerebral Cortex*. Edited by L. C. Triarhou. Karger. Available at: https://www.karger.com/Book/Home/247637 (Accessed: 16 January 2021).

ENIGMA Clinical High Risk for Psychosis Working Group *et al.* (2021) 'Association of Structural Magnetic Resonance Imaging Measures With Psychosis Onset in Individuals at Clinical High Risk for Developing Psychosis: An ENIGMA Working Group Mega-analysis', *JAMA psychiatry*. doi: 10.1001/jamapsychiatry.2021.0638.

van Erp, T. G. M. *et al.* (2018) 'Cortical Brain Abnormalities in 4474 Individuals With Schizophrenia and 5098 Control Subjects via the Enhancing Neuro Imaging Genetics Through Meta Analysis (ENIGMA) Consortium', *Biological Psychiatry*, 84(9), pp. 644–654. doi: 10.1016/j.biopsych.2018.04.023.

Feinberg, I. (1982) 'Schizophrenia: Caused by a fault in programmed synaptic elimination during adolescence?', *Journal of Psychiatric Research*, 17(4), pp. 319–334. doi: 10.1016/0022-3956(82)90038-3.

French, L. *et al.* (2015) 'Early Cannabis Use, Polygenic Risk Score for Schizophrenia, and Brain Maturation in Adolescence', *JAMA psychiatry*, 72(10), pp. 1002–1011. doi: 10.1001/jamapsychiatry.2015.1131.

García-Cabezas, M. Á. *et al.* (2017) 'Mirror trends of plasticity and stability indicators in primate prefrontal cortex', *European Journal of Neuroscience*, 46(8), pp. 2392–2405. doi: https://doi.org/10.1111/ejn.13706.

García-Cabezas, M. Á., Hacker, J. L. and Zikopoulos, B. (2020) 'A Protocol for Cortical Type Analysis of the Human Neocortex Applied on Histological Samples, the Atlas of Von

Economo and Koskinas, and Magnetic Resonance Imaging', *Frontiers in Neuroanatomy*, 14. doi: 10.3389/fnana.2020.576015.

The Gene Ontology Consortium (2019) 'The Gene Ontology Resource: 20 years and still GOing strong', *Nucleic Acids Research*, 47(D1), pp. D330–D338. doi: 10.1093/nar/gky1055.

Giedd, J. N. *et al.* (1999) 'Brain development during childhood and adolescence: a longitudinal MRI study', *Nature Neuroscience*, 2(10), pp. 861–863. doi: 10.1038/13158.

Gogtay, N. *et al.* (2004) 'Dynamic mapping of human cortical development during childhood through early adulthood', *Proceedings of the National Academy of Sciences*, 101(21), pp. 8174–8179. doi: 10.1073/pnas.0402680101.

Hayasaka, S. *et al.* (2004) 'Nonstationary cluster-size inference with random field and permutation methods', *NeuroImage*, 22(2), pp. 676–687. doi: 10.1016/j.neuroimage.2004.01.041.

Herculano-Houzel, S., Watson, C. R. and Paxinos, G. (2013) 'Distribution of neurons in functional areas of the mouse cerebral cortex reveals quantitatively different cortical zones', *Frontiers in Neuroanatomy*, 7. doi: 10.3389/fnana.2013.00035.

Hibar, D. P. *et al.* (2018) 'Cortical abnormalities in bipolar disorder: an MRI analysis of 6503 individuals from the ENIGMA Bipolar Disorder Working Group', *Molecular Psychiatry*, 23(4), pp. 932–942. doi: 10.1038/mp.2017.73.

Hoogman, M. *et al.* (2019) 'Brain Imaging of the Cortex in ADHD: A Coordinated Analysis of Large-Scale Clinical and Population-Based Samples', *American Journal of Psychiatry*, 176(7), pp. 531–542. doi: 10.1176/appi.ajp.2019.18091033.

Huntenburg, J. M. *et al.* (2017) 'A Systematic Relationship Between Functional Connectivity and Intracortical Myelin in the Human Cerebral Cortex', *Cerebral Cortex*, 27(2), pp. 981–997. doi: 10.1093/cercor/bhx030.

Insel, T. R. (2010) 'Rethinking schizophrenia', *Nature*, 468(7321), pp. 187–193. doi: 10.1038/nature09552.

Jernigan, T. L. *et al.* (2016) 'The Pediatric Imaging, Neurocognition, and Genetics (PING) Data Repository', *NeuroImage*, 124, pp. 1149–1154. doi: 10.1016/j.neuroimage.2015.04.057.

Kang, H. J. *et al.* (2011) 'Spatio-temporal transcriptome of the human brain', *Nature*, 478(7370), pp. 483–489. doi: 10.1038/nature10523.

Kessler, R. C. *et al.* (2007) 'Lifetime prevalence and age-of-onset distributions of mental disorders in the World Health Organization's World Mental Health Survey Initiative', *World psychiatry: official journal of the World Psychiatric Association (WPA)*, 6(3), pp. 168–176.

Khundrakpam, B. *et al.* (2020) 'Neural correlates of polygenic risk score for autism spectrum disorders in general population', *Brain Communications*, 2(2). doi: 10.1093/braincomms/fcaa092.

Khundrakpam, B. S. *et al.* (2017) 'Cortical Thickness Abnormalities in Autism Spectrum Disorders Through Late Childhood, Adolescence, and Adulthood: A Large-Scale MRI

Study', *Cerebral Cortex (New York, N.Y.: 1991)*, 27(3), pp. 1721–1731. doi: 10.1093/cercor/bhx038.

Kirov, G. *et al.* (2012) 'De novo CNV analysis implicates specific abnormalities of postsynaptic signalling complexes in the pathogenesis of schizophrenia', *Molecular Psychiatry*, 17(2), pp. 142–153. doi: 10.1038/mp.2011.154.

Kirschner, M. *et al.* (2020) 'Latent Clinical-Anatomical Dimensions of Schizophrenia', *Schizophrenia Bulletin*. doi: 10.1093/schbul/sbaa097.

Kirschner, M. *et al.* (2021) 'Cortical and Subcortical Neuroanatomical Signatures of Schizotypy in 3,004 Individuals Assessed in a Worldwide ENIGMA Study', *medRxiv*, p. 2021.04.29.21255609. doi: 10.1101/2021.04.29.21255609.

Klingler, E. *et al.* (2021) 'Mapping the molecular and cellular complexity of cortical malformations', *Science*, 371(6527). doi: 10.1126/science.aba4517.

Larivière, S. *et al.* (2020) 'Network-based atrophy modeling in the common epilepsies: A worldwide ENIGMA study', *Science Advances*, 6(47), p. eabc6457. doi: 10.1126/sciadv.abc6457.

Lariviere, S. *et al.* (2020) 'The ENIGMA Toolbox: Cross-disorder integration and multiscale neural contextualization of multisite neuroimaging datasets', *bioRxiv*, p. 2020.12.21.423838. doi: 10.1101/2020.12.21.423838.

Liu, B. *et al.* (2017) 'Polygenic Risk for Schizophrenia Influences Cortical Gyrification in 2 Independent General Populations', *Schizophrenia Bulletin*, 43(3), pp. 673–680. doi: 10.1093/schbul/sbw051.

Margulies, D. S. *et al.* (2016) 'Situating the default-mode network along a principal gradient of macroscale cortical organization', *Proceedings of the National Academy of Sciences*, 113(44), pp. 12574–12579. doi: 10.1073/pnas.1608282113.

Markello, R. D. and Misic, B. (2020) 'Comparing spatially-constrained null models for parcellated brain maps', *bioRxiv*, p. 2020.08.13.249797. doi: 10.1101/2020.08.13.249797.

McCarthy, S. *et al.* (2016) 'A reference panel of 64,976 haplotypes for genotype imputation', *Nature Genetics*, 48(10), pp. 1279–1283. doi: 10.1038/ng.3643.

Neilson, E. *et al.* (2017) 'Effects of environmental risks and polygenic loading for schizophrenia on cortical thickness', *Schizophrenia Research*, 184, pp. 128–136. doi: 10.1016/j.schres.2016.12.011.

Neilson, E. *et al.* (2019) 'Impact of Polygenic Risk for Schizophrenia on Cortical Structure in UK Biobank', *Biological Psychiatry*. doi: 10.1016/j.biopsych.2019.04.013.

Opel, N. *et al.* (2020) 'Cross-Disorder Analysis of Brain Structural Abnormalities in Six Major Psychiatric Disorders: A Secondary Analysis of Mega- and Meta-analytical Findings From the ENIGMA Consortium', *Biological Psychiatry*, 0(0). doi: 10.1016/j.biopsych.2020.04.027.

Pantelis, C. *et al.* (2003) 'Neuroanatomical abnormalities before and after onset of psychosis: a cross-sectional and longitudinal MRI comparison', *Lancet (London, England)*, 361(9354), pp. 281–288. doi: 10.1016/S0140-6736(03)12323-9.

Paquola, C., Wael, R. V. D., *et al.* (2019) 'Microstructural and functional gradients are increasingly dissociated in transmodal cortices', *PLOS Biology*, 17(5), p. e3000284. doi: 10.1371/journal.pbio.3000284.

Paquola, C., Bethlehem, R. A., *et al.* (2019) 'Shifts in myeloarchitecture characterise adolescent development of cortical gradients', *eLife*. Edited by J. I. Gold et al., 8, p. e50482. doi: 10.7554/eLife.50482.

Paquola, C. *et al.* (2020) 'A multi-scale cortical wiring space links cellular architecture and functional dynamics in the human brain', *PLOS Biology*, 18(11), p. e3000979. doi: 10.1371/journal.pbio.3000979.

Park, B. *et al.* (2021) 'An expanding manifold in transmodal regions characterizes adolescent reconfiguration of structural connectome organization', *eLife*. Edited by L. Q. Uddin, T. E. Behrens, and B. D. Fulcher, 10, p. e64694. doi: 10.7554/eLife.64694.

Rapoport, J. L., Giedd, J. N. and Gogtay, N. (2012) 'Neurodevelopmental model of schizophrenia: update 2012', *Molecular Psychiatry*, 17(12), pp. 1228–1238. doi: 10.1038/mp.2012.23.

Raznahan, A. *et al.* (2011) 'How Does Your Cortex Grow?', *The Journal of Neuroscience*, 31(19), pp. 7174–7177. doi: 10.1523/JNEUROSCI.0054-11.2011.

ReproGen Consortium *et al.* (2015) 'An atlas of genetic correlations across human diseases and traits', *Nature Genetics*, 47(11), pp. 1236–1241. doi: 10.1038/ng.3406.

Reus, L. M. *et al.* (2017) 'Association of polygenic risk for major psychiatric illness with subcortical volumes and white matter integrity in UK Biobank', *Scientific Reports*, 7. doi: 10.1038/srep42140.

van Rooij, D. *et al.* (2018) 'Cortical and Subcortical Brain Morphometry Differences Between Patients With Autism Spectrum Disorder and Healthy Individuals Across the Lifespan: Results From the ENIGMA ASD Working Group', *The American Journal of Psychiatry*, 175(4), pp. 359–369. doi: 10.1176/appi.ajp.2017.17010100.

Ruderfer, D. M. *et al.* (2018) 'Genomic Dissection of Bipolar Disorder and Schizophrenia, Including 28 Subphenotypes', *Cell*, 173(7), pp. 1705-1715.e16. doi: 10.1016/j.cell.2018.05.046.

Sanides, F. (1962) '[Architectonics of the human frontal lobe of the brain. With a demonstration of the principles of its formation as a reflection of phylogenetic differentiation of the cerebral cortex]', *Monographien Aus Dem Gesamtgebiete Der Neurologie Und Psychiatrie*, 98, pp. 1–201.

Schizophrenia Working Group of the Psychiatric Genomics Consortium *et al.* (2014) 'Biological insights from 108 schizophrenia-associated genetic loci', *Nature*, 511(7510), pp. 421–427. doi: 10.1038/nature13595.

Schmaal, L. *et al.* (2017) 'Cortical abnormalities in adults and adolescents with major depression based on brain scans from 20 cohorts worldwide in the ENIGMA Major Depressive Disorder Working Group', *Molecular Psychiatry*, 22(6), pp. 900–909. doi: 10.1038/mp.2016.60.

Schmitt, J. E. *et al.* (2014) 'The dynamic role of genetics on cortical patterning during childhood and adolescence', *Proceedings of the National Academy of Sciences of the United States of America*, 111(18), pp. 6774–6779. doi: 10.1073/pnas.1311630111.

Seidlitz, J. *et al.* (2020) 'Transcriptomic and cellular decoding of regional brain vulnerability to neurogenetic disorders', *Nature Communications*, 11(1), p. 3358. doi: 10.1038/s41467-020-17051-5.

Sellgren, C. M. *et al.* (2019) 'Increased synapse elimination by microglia in schizophrenia patient-derived models of synaptic pruning', *Nature Neuroscience*, 22(3), pp. 374–385. doi: 10.1038/s41593-018-0334-7.

Shaw, P. *et al.* (2006) 'Intellectual ability and cortical development in children and adolescents', *Nature*, 440(7084), pp. 676–679. doi: 10.1038/nature04513.

Shaw, P. *et al.* (2007) 'Attention-deficit/hyperactivity disorder is characterized by a delay in cortical maturation', *Proceedings of the National Academy of Sciences of the United States of America*, 104(49), pp. 19649–19654. doi: 10.1073/pnas.0707741104.

Sotiras, A. *et al.* (2017) 'Patterns of coordinated cortical remodeling during adolescence and their associations with functional specialization and evolutionary expansion', *Proceedings of the National Academy of Sciences*, 114(13), pp. 3527–3532. doi: 10.1073/pnas.1620928114.

Sowell, E. R. *et al.* (2004) 'Longitudinal Mapping of Cortical Thickness and Brain Growth in Normal Children', *Journal of Neuroscience*, 24(38), pp. 8223–8231. doi: 10.1523/JNEUROSCI.1798-04.2004.

Sprooten, E. *et al.* (2019) 'Depth-dependent intracortical myelin organization in the living human brain determined by in vivo ultra-high field magnetic resonance imaging', *NeuroImage*, 185, pp. 27–34. doi: 10.1016/j.neuroimage.2018.10.023.

Srinivas, K. V. *et al.* (2017) 'The Dendrites of CA2 and CA1 Pyramidal Neurons Differentially Regulate Information Flow in the Cortico-Hippocampal Circuit', *Journal of Neuroscience*, 37(12), pp. 3276–3293. doi: 10.1523/JNEUROSCI.2219-16.2017.

Sun, D. *et al.* (2018) 'Large-scale mapping of cortical alterations in 22q11.2 deletion syndrome: Convergence with idiopathic psychosis and effects of deletion size', *Molecular Psychiatry*, pp. 1–13. doi: 10.1038/s41380-018-0078-5.

Tamnes, C. K. *et al.* (2017) 'Development of the Cerebral Cortex across Adolescence: A Multisample Study of Inter-Related Longitudinal Changes in Cortical Volume, Surface Area, and Thickness', *The Journal of Neuroscience: The Official Journal of the Society for Neuroscience*, 37(12), pp. 3402–3412. doi: 10.1523/JNEUROSCI.3302-16.2017.

Van der Auwera, S. *et al.* (2015) 'No association between polygenic risk for schizophrenia and brain volume in the general population', *Biological Psychiatry*, 78(11), pp. e41-42. doi: 10.1016/j.biopsych.2015.02.038.

Wannan, C. M. J. *et al.* (2019) 'Evidence for Network-Based Cortical Thickness Reductions in Schizophrenia', *The American Journal of Psychiatry*, 176(7), pp. 552–563. doi: 10.1176/appi.ajp.2019.18040380.

Wei, W. *et al.* (2020) 'Depth-dependent abnormal cortical myelination in first-episode treatment-naïve schizophrenia', *Human Brain Mapping*, 41(10), pp. 2782–2793. doi: https://doi.org/10.1002/hbm.24977.

Wierenga, L. M. *et al.* (2014) 'Unique developmental trajectories of cortical thickness and surface area', *NeuroImage*, 87, pp. 120–126. doi: 10.1016/j.neuroimage.2013.11.010.

Worsley, K. *et al.* (2009) 'SurfStat: A Matlab toolbox for the statistical analysis of univariate and multivariate surface and volumetric data using linear mixed effects models and random field theory', *NeuroImage*, 47, p. S102. doi: 10.1016/S1053-8119(09)70882-1.

Worsley, K. J. *et al.* (2004) 'Unified univariate and multivariate random field theory', *NeuroImage*, 23, pp. S189–S195. doi: 10.1016/j.neuroimage.2004.07.026.

Writing Committee for the Attention-Deficit/Hyperactivity Disorder *et al.* (2021) 'Virtual Histology of Cortical Thickness and Shared Neurobiology in 6 Psychiatric Disorders', *JAMA Psychiatry*, 78(1), pp. 47–63. doi: 10.1001/jamapsychiatry.2020.2694.

Zhu, Y. *et al.* (2018) 'Spatiotemporal transcriptomic divergence across human and macaque brain development', *Science*, 362(6420). doi: 10.1126/science.aat8077.

Zielinski, B. A. *et al.* (2014) 'Longitudinal changes in cortical thickness in autism and typical development', *Brain*, 137(6), pp. 1799–1812. doi: 10.1093/brain/awu083.

Tables

Table 1. Sample Characteristics

Variables	Sample (n=390)
Age, mean (SD)	12.10 (4.77)
Gender (%)	46.80 % female
Handedness (n=390)	left=38; right=338; mixed=14
Socioeconomic Status, mean (SD)	11.76 (1.89)
Family History (%)	
Schizophrenia family risk	0.056
Bipolar family risk	0.171
Depression&Anxiety family risk	0.529
ADHD family risk	0.256

Supplementary Materials

Image acquisition and pre-processing

The CIVET processing pipeline, (http://www.bic.mni.mcgill.ca/ServicesSoftware/CIVET) involved the following steps: T1-weighted image were first non-uniformity corrected, and then linearly registered to the Talairach-like MNI152 template (established with the ICBM152 dataset). Using the template mask, the non-uniformity correction was repeated. In a next step, the non-linear registration from the resulting volume to the MNI152 template was computed priors were obtained from the transform to segment the image into GM, WM, and cerebrospinal fluid. Inner and outer GM surfaces were then extracted using the Constrained Laplacian-based Automated Segmentation with Proximities (CLASP) algorithm, and cortical thickness was estimated in native space using the linked distance between the two surfaces at 81,924 vertices. Each subject's cortical thickness map was blurred using a 30-millimeter full width at half maximum surface-based diffusion smoothing kernel to impose a normal distribution on the corticometric data, and to increase the signal to noise ratio.

Model selection

The corrected Akaike information criterion (AIC) (Akaike, 1969; HURVICH and TSAI, 1989) and Bayesian information criterion (BIC) (Schwarz, 1978) were used to test whether models including quadratic age terms and interaction terms fit the data better than models with only lower degree age terms. The following three models were compared.

Model 1: including quadratic age terms and PRS-SCZ*age interaction terms (β_4PRS-SCZ*Age + β_5PRS-SCZ*Age$^{2)}$

$$T_i = intercept + \beta_1 PRS\text{-}SCZ + \beta_2 Age + \beta_3 Age^2 + \beta_4 PRS\text{-}SCZ{*}Age + \beta_5 PRS\text{-}SCZ{*}Age^2 + \beta_6 Sex + \beta_7 PC10 + \beta_8 Scanner + \beta_9 BrainVolume + \varepsilon_i$$

Model 2: without quadratic age terms but including one PRS-SCZ*age interaction term (β_4PRS-SCZ*Age)

$$T_i = intercept + \beta_1 PRS\text{-}SCZ + \beta_2 Age + \beta_3 PRS\text{-}SCZ{*}Age + \beta_4 Sex + \beta_5 PC10 + \beta_6 Scanner + \beta_7 BrainVolume + \varepsilon_i$$

Model 3: including quadratic age terms but excluding PRS-SCZ*age interaction terms

$$T_i = intercept + \beta_1 PRS\text{-}SCZ + \beta_2 Age + \beta_3 Age^2 + \beta_4 Sex + \beta_5 PC10 + \beta_6 Scanner + \beta_7 BrainVolume + \varepsilon_i$$

Model	corrected AIC	BIC
Model 1 Age ^{2} + interaction terms	-909.25	1.0e+03 *-1267.1
Model 2 Age + interaction terms	-902.59	1.0e+03 *-1256.6
Model 3 Age^2 without interaction terms	-904.47	1.0e+03 *-1258.5

The corrected AIC and BIC values indicated that model 1 including quadratic age terms and PRS-SCZ*age, PRS-SCZ*age^2 showed the best model fit for the data.

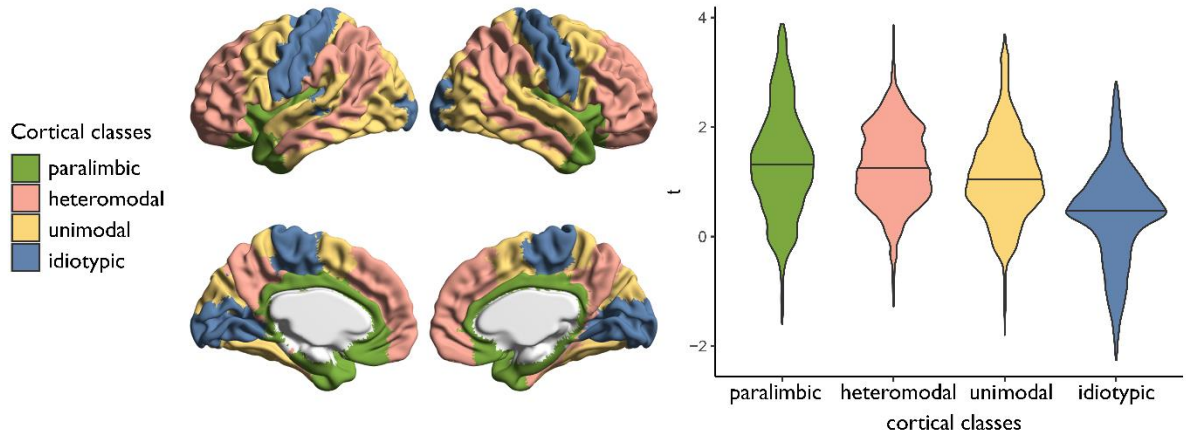

Supplementary Figure 1: Stratification of t-statistics (Figure 1) by cortical class, which reflect differences in modality specificity and laminar differentiation (Mesulam, 1998). Association cortex, which includes paralimbic, heteromodal and unimodal classes, harbor higher t-values than the idiotypic sensory cortex.

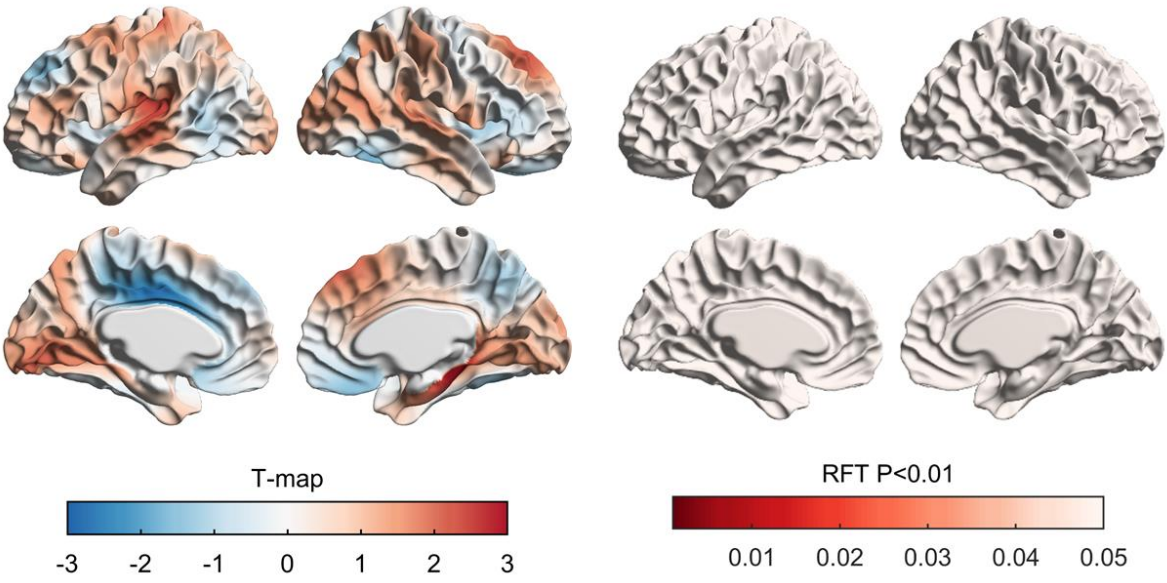

Supplementary Figure 2: C) Unthresholded (left) and cluster-level thresholded (right) maps show the association of PRS-SCZ with surface area using Random field theory (RFT) at cluster-level $p \leq .01$ (Hayasaka *et al.*, 2004; Worsley *et al.*, 2004).

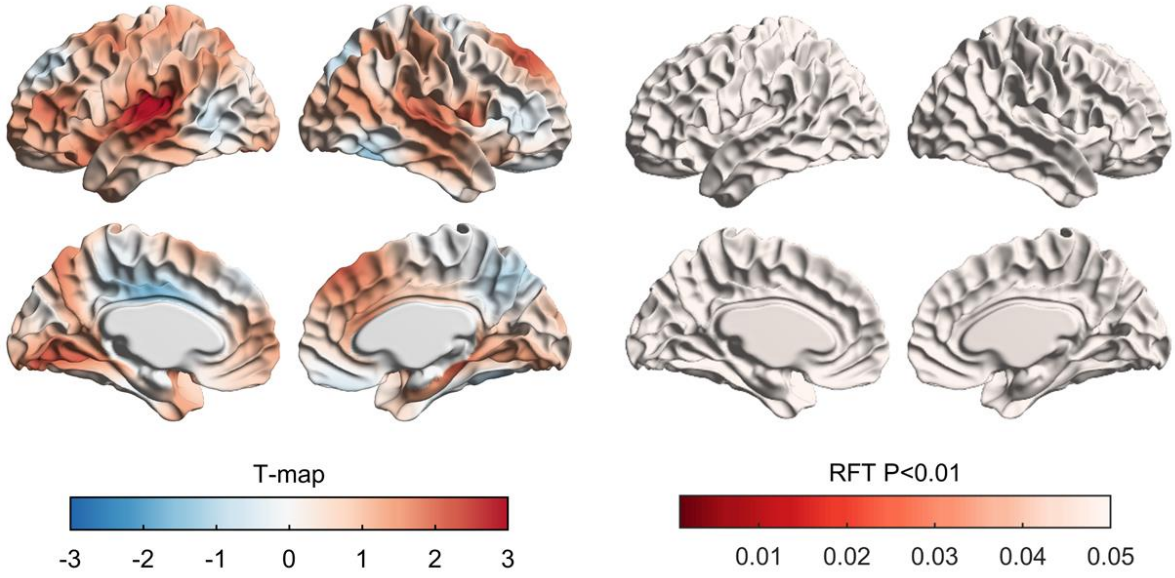

Supplementary Figure 3: Unthresholded (left) and cluster-level thresholded (right) maps show the association of PRS-SCZ with cortical volume using Random field theory (RFT) at cluster-level $p \leq .01$ (Hayasaka *et al.*, 2004; Worsley *et al.*, 2004).

.

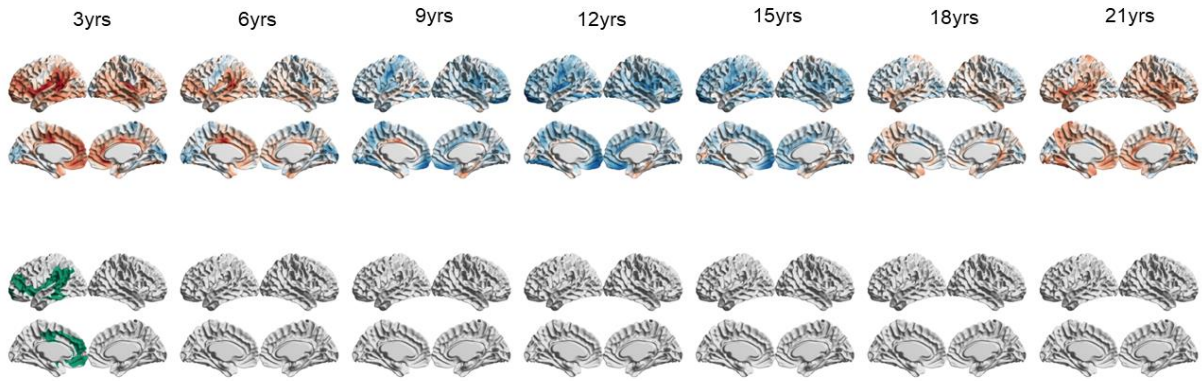

Supplementary Figure S4: Age-specific PRS-SCZ effect on cortical thickness Age 3 to 21. Upper row unthresholed maps of PRS-SCZ effect on cortical thickness with different age-centering. Lower row cluster-level thresholded maps of PRS-SCZ effect on cortical thickness with different age-centering using Random field theory (RFT) at cluster-level $p \leq .05$ (Hayasaka *et al.*, 2004; Worsley *et al.*, 2004).

Age 3 to 9

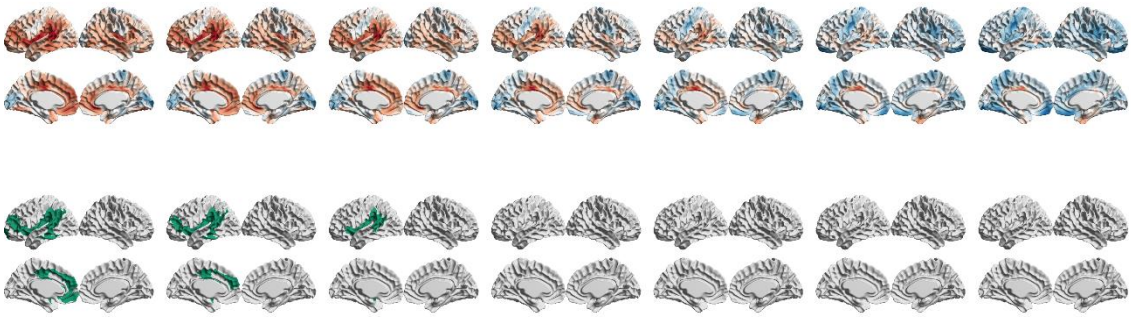

Age 10 to 16

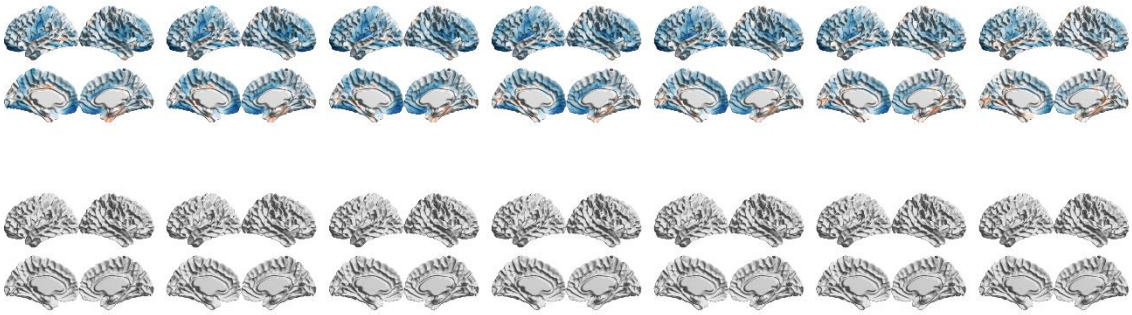

Age 17 to 21

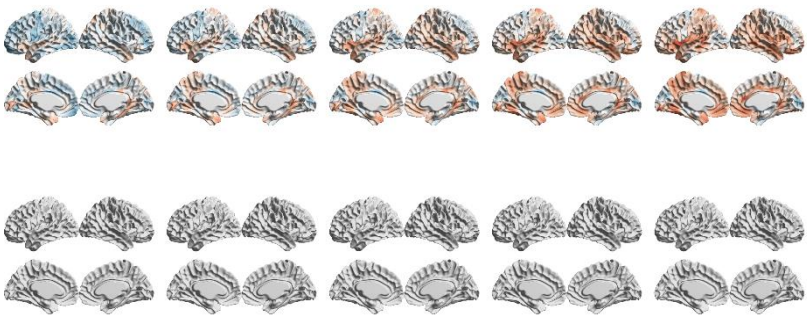

Supplementary Figure S5: Age-specific PRS-SCZ effect on cortical thickness Age 3 to 21 showing all 21 age bins. Upper rows unthresholed maps of PRS-SCZ effect on cortical thickness with different age-centering. Lower rows cluster-level thresholded maps of PRS-SCZ effect on cortical thickness with different age-centering using Random field theory